RSC Advances

This is an *Accepted Manuscript*, which has been through the Royal Society of Chemistry peer review process and has been accepted for publication.

Accepted Manuscripts are published online shortly after acceptance, before technical editing, formatting and proof reading. Using this free service, authors can make their results available to the community, in citable form, before we publish the edited article. This *Accepted Manuscript* will be replaced by the edited, formatted and paginated article as soon as this is available.

You can find more information about *Accepted Manuscripts* in the Information for Authors.

Please note that technical editing may introduce minor changes to the text and/or graphics, which may alter content. The journal's standard Terms & Conditions and the Ethical guidelines still apply. In no event shall the Royal Society of Chemistry be held responsible for any errors or omissions in this *Accepted Manuscript* or any consequences arising from the use of any information it contains.

ROYAL SOCIETY OF CHEMISTRY

www.rsc.org/advances

Please do not adjust margins

RSC Advances

PAPER

Probing into Highly Transparent and Conducting SnO_x /Au/SnO_x Structure for Futuristic TCO Applications

V. Sharma,[a] R. Vyas,[b] P. Bazylewski,[c] G. S. Chang,[d] K. Asokan,[e] and K. Sachdev[a,f]

Received 00th November 20xx,
Accepted 00th December 20xx

DOI: 10.1039/x0xx00000x

www.rsc.org/

The SnO_x/Au/SnO_x transparent conductive oxide (TCO) multilayered film was fabricated with a total thickness of 75 nm using both e-beam and thermal evaporation techniques. X-ray diffraction confirms the amorphous nature of SnO_x with a crystalline peak attributed to the presence of diffraction from Au (111) plane. The morphological studies using Atomic force microscopy (AFM) and Scanning electron microscopy (SEM) revealed a smooth top layer of the sandwich structure. Rutherford backscattering spectrumhas been used to probe the thickness of individual TCO layers, and reveals an oxygen deficient structure in the SnO_x layer. X-ray absorption spectroscopy (XAS) and X-ray emission spectroscopy (XES) measurements confirm the formation an SnO-rich phase and the presence of oxygen vacancies.The specimen exhibited resistivity and sheet resistance of $3.9\times10^{-4}\Omega\cdot$cm and 52 Ω/*sq.*, respectively with an optical transparency of 83% beyond 475nm. The superior parameters exhibited by this stacked multilayer are due to relatively less oxygen concentration in the tin oxide layer and it is therefore proposed as necessary ingredient to increase the overall conductivity in metal oxide multilayer thin film.

Introduction

There has been a growing need of transparent conducting oxides (TCOs) to support photovoltaic and optoelectronic applications. Various TCOs have been developed scaling from very simplistic structures[1] to the most complicated hetero-structures.[2-4] Such structures have already been in discussion and later discarded for their complex counterparts offering high conductivity, transparency and stability but at a cost of complex manufacturing procedures. The quest for research in TCOs has led to the development of a coating with (1) superior transparency in visible region, (2) excellent conducting properties and (3) better temperature and mechanical stability. The optimization of transparency and conductivity has always presented a roadblock for the development of efficient TCOs.

In recent years, the efficiency of transparent oxides has improved to some extent but requires more research.[4] The conductivity of these metal oxides is limited by the scattering due to coulomb interaction between ionized donor and free electrons.[5] This puts a limit to the TCO conductivity as $4\times10^{-4}\Omega\cdot cm$.[6-8] Among various structures, stacked multilayer thin films have proved to be suitable candidates. It is well known that thickness of metal oxide and noble metal layer play an important role in tuning the electrical conductivity and optical properties of the stacked multilayer. The thickness of metal layer below 20 nm increases the transparency as well as charge transport.[9] It is reported that *Au* metal is more effective in increasing conductivity and transparency.[10] Due to the high cost (Indium bar price 99.99% ≈ $1000 per 100g) and relatively limited availability of indium in nature, the research for alternatives to ITO is in progress.

One of such alternatives is tin oxide which offers a higher conductivity even at ultrathin thickness[11-12] which is necessary for it to be realized as a candidate for TCO applications. In this aspect, a tri-layered structure has been reported by Bou *et al.*[13] which describes the use of indium-tin-oxide (ITO) free SnO_x/Au/SnO_x for organic photovoltaic application. It is reported that the sheet resistance is 6.7 Ω/*sq.* with a transparency of 67% which are comparable to the values of ITO films. Yu *et al.*[14] also reported such tri-layered structure with *Ag* as sandwich layer (SnO_2/Ag/SnO_2) offering sheet resistance of 9.61 Ω/*sq.*, resistivity of $4.8\times10^{-5}\Omega\cdot cm$ and transmittance of more than 83% in the visible region.

In addition to the material and design of multilayer structure, the device performance is known to be dictated conclusively by the surface morphology of TCO especially for display[15-16] and energy conversion applications like OLED or OPV.[17] There have been reports on the role of surface roughness as one of the influencing factors in determining the efficiency of TCO electrodes.[15] Films with higher roughness are known to show less transparency as a result of scattering of light due to the

[a.] Department of Physics, Malaviya National Institute of Technology, Jaipur-302017 India. Email: phyvikas@gmail.com
[b.] Department of Physics, School of Basic Sciences, Jaipur National University, Jaipur-302017 India.
[c.] Department of Physics & Astronomy, University of Western, Ontario, London-N6A 3K7 Canada.
[d.] Department of Physics & Engineering Physics, University of Saskatchewan, Saskatoon-S7N 5E2 Canada.
[e.] Materials Science Division, Inter-University Accelerator Centre, New Delhi-110067, India.
[f.] Materials Research Centre, Malaviya National Institute of Technology, Jaipur-302017 India.ksachdev.phy@mnit.ac.in

RSC Advances Accepted Manuscript

rough surface.[16] In the case of organic electronic devices, control over surface roughness of the TCO is a serious concern. Two or more organic active layers are to be deposited on the TCO and a poor interfacial adherence between top surface and the next organic active layer is detrimental to the device performance.[17]

X-ray absorption spectroscopy (XAS) and X-ray emission spectroscopy (XES) have been used extensively in recent years for probing the electronic structure of materials.[18-21] In case of XAS, the absorption of an X-ray by one of the core electrons results in the electron being excited to a higher energy unoccupied state or ejected from the atom thereby creating a core hole. XAS is useful in studying the local atomic environment and analyzing materials based on their characteristic X-ray absorption edge. In X-ray emission, the incident X-ray knocks out a core electron. The core hole is filled by a valence electron and a photon is emitted and can be detected to provide a measure of the valence band states, complimentary to XAS. XAS studies have been used to investigate the effect of Ag doping on the electronic structure of In_2O_3 films and have reported an increase in the density of conduction band states in the O K-edge spectrum.[20]This has been attributed to the orbital overlap between the O-2*p* and Ag-4*d* and Ag-5*sp* orbitals, which may result in increased electron carrier transport.[20]Kapilashrami*et. al*[21] have used the XAS and XES spectra to determine the band gap of $Zn_{1-x}Sn_xO$ thin films.

In the present manuscript, the focus is to revive the discussion on conventional process by designing a multilayer structure for better TCO properties. For this, e-beam evaporation was used to create a mixed phase of SnO/SnO_2 with reduced oxygen during deposition due to vacuum drag to increase the conductivity of metal oxide layer. This study also aims to increase the transmittance of multilayered films over the reported transmittance[13-14] using a high performing stacked multilayered structure of $SnO_x/Au/SnO_x$ for various technological applications.

Experimental details

Sample Preparation

SnO_2 powder (Alfa-Aesar, 99.999% of purity, metal basis) is used as starting material for making pellet for e-beam evaporation. SnO_2 powder was subjected to grinding and pelletized. These pellets were then sintered at 500°C for 3 hrs to get better structural stability for film deposition.

The quartz substrates of 1x1 cm^2 were cleaned using standard cleaning processes and kept in iso-propanol. These substrates were then given a heat treatment at 200 °C prior to deposition to remove any organic impurity on the surface. The stacked multilayer was then deposited on these quartz substrates using e-beam evaporation (for SnO_2 layer) and thermal evaporation (for Au layer) techniques at room temperature. SnO_2 films were deposited keeping the evaporation parameters as: source to substrate distance - 16 cm, base pressure 7×10^{-7} mbar, working pressure 1.4×10^{-5} mbar, rate of deposition 0.2 nm/sec, voltage 200 V and current 10 mA. The Au layer was deposited using thermal evaporation unit with base pressure 8×10^{-7} mbar, working pressure 1.4×10^{-6} mbar, voltage1V, current 280 A and deposition rate of 0.1nm/sec to deposit a thickness of 5 nm. The process of SnO_2 film deposition is then repeated to deposit the 35nm thick uppermost layer making the total thickness of the multilayered structure as 75 nm.

The resultant $SnO_x/Au/SnO_x$ stacked multilayer was annealed in open air furnace at various temperatures (30-150°C) to test the thermal stability of multilayered structure. These thin films annealed at different temperature then checked by X-ray diffraction. All other measurements were carried out for the as deposited $SnO_x/Au/SnO_x$ stacked multilayer at room temperature.

Characterization

X-ray diffraction (XRD) measurement of the sample was carried out using a Bruker D8 Advance X-ray diffractometer. The field-emission scanning electron microscopy (FE-SEM) and atomic force microscopy (AFM) images were collected using Nova Nano FESEM 450 (FEI) and NanoscopeIIIa, respectively. UV-Vis spectrum of the sample was obtained using LAMBDA 750 (Perkin Elmer) UV-Vis NIR spectrophotometer. The Raman spectrum of specimen was taken using Renishaw Raman spectrometer with Ar ion laser with 514.5 nm wavelength and 50 mW power.

The low temperature Hall measurements were performed using a variable temperature Hall set up (model HMS 5500) from Ecopia Co., Korea. The current-voltage characteristics were measured using a custom built setup consisting of a cryostat controlled with Lakeshore 325 temperature controller and Keithley 2400 SMU.

The interface was investigated with Rutherford backscattering (RBS) spectrometry using 2 MeV He^+ ion beams at Inter-University Accelerator Centre, New Delhi (India). Measurement of O*K*-edge and Sn *M*-edge XAS and XES were performed at Resonant Elastic and Inelastic scattering (REIXS) beamline of Canadian Light Source (CLS), Canada. XAS spectra were obtained in both surface sensitive total electron yield (TEY) and bulk-sensitive total fluorescence yield (TFY) modes using linearly polarized X-rays at a 45° angle of incidence. Non-resonant XES measurements of the O *K*-edge were collected by exciting above the absorption edge at 560 eV.

Results and Discussion

X-ray diffraction study

The glancing angle X-ray diffraction curve for room temperature $SnO_x/Au/SnO_x$ staked multilayer specimen(shown in fig.1a) is suggestive of formation of amorphous metal oxide with multiple peaks at 38.18°, 44.39°, 64.57° and 77.54° corresponding to the Au cubic crystal planes of 111, 200, 220 and 311, respectively(JCPDS-card no. 00-004-0784).

The high intensity background counts in the top curve of fig.1a (shown with exponential fit) is due to amorphous nature of SnO_x

RSC Advances Accepted Manuscript

 This journal is © The Royal Society of Chemistry 20xx

and SiO_2 (substrate) layer. The bottom curve of the fig.1a shows the residue of the fit after subtracting the exponential fit data from the obtained spectrum.

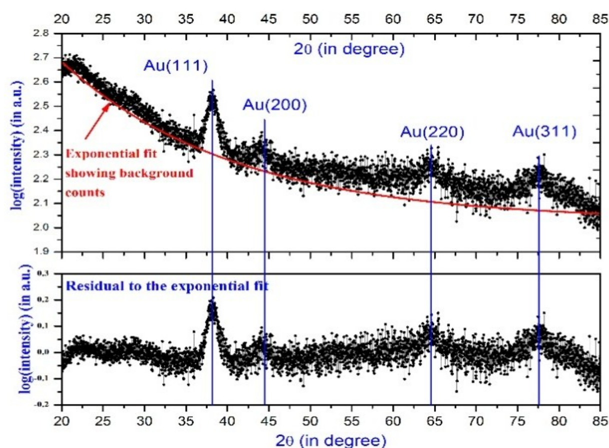

Fig. 1a X-ray diffraction pattern of as-deposited SnO_x/Au/SnO_x staked multilayer.

The diffraction patterns were also recorded for the staked layer annealed at various temperatures and are shown in fig. 1 b which indicates the formation of an amorphous phase except an intense peak at 2θ ≈ 38.04°corresponding to Au (111) plane. We note that there is no change in the intensities and the peak positions with annealing temperatures. This confirms the stability of multilayer structure in the temperature range of photovoltaic and optoelectronic device operation, i.e., room temperature to 150°C.

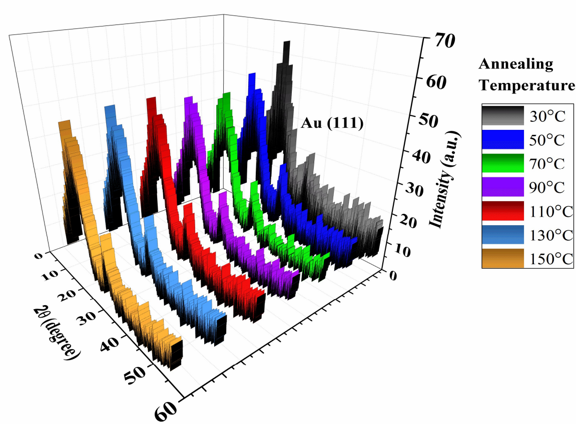

Fig.1 (b) X-ray diffraction pattern showing amorphous nature of stacked multilayers with annealing temperatures

Such amorphous film is advantageous for growth of various films due to absence of lattice mismatch between the hetero-layers. A similar result of amorphous metal oxide film with crystalline metal as sandwich layer has been reported by Lee *et al.* [10]

Morphological studies

Surface morphology of the stacked multilayer was investigated by FE-SEM and AFM, and the results are presented in Fig.2 (a-b). Both images suggest the formation of relatively flat films with randomly distributed islands with atypical dimension of nms. The size distribution of islands from FE-SEM image was analyzed using particle fitting tool of ImageJ[22] (assuming circular shape of islands on the surface) and the radius of islands was determined to be in a range from 5 nm to 60 nm with an average radius of about 20 nm.

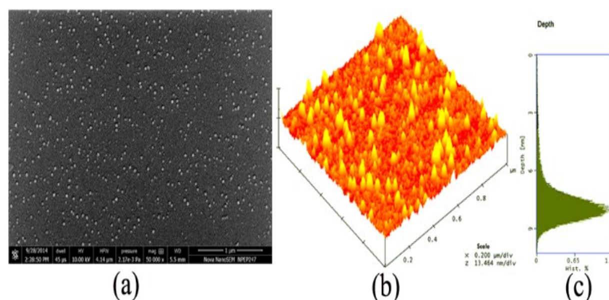

Fig.2 (a) SEM image exhibiting a flat topology of stacked multilayer (b) AFM image showing the surface topology of sandwich layer along with (c) depth histogram.

Fig. 2(b-c)shows the AFM image of multilayer (fig. 2b) and the depth-distribution curve (fig. 2c)which exhibits a maximum depth of around 7.5 nm and a maximum height of 11.64 nm when analyzed with Nanoscope™version-5.31R1. The average particle size distribution was also employed on 2D AFM scan assuming spherical particle on the film surface. This analysis showed that these particles have a radius from 5 nm to 60 nm with a mean radius of about 28 nm which are consistent with results from FE-SEM analysis.[22]
The root-mean-square roughness of the stacked multilayer has been also calculated and found to be 1.184 nm. The small roughness is a necessary requirement for such stacked multilayered film for their use as substrate for optoelectronic applications.[15]
The estimation of Au has also been performed using Energy dispersive x-ray spectroscopy (EDS) and is given under supplementary information (see fig. S1 with Si and fig. S2 after ignoring Si). The tables showing the relative contents of elements are also appended as table TS1 and table TS2 which suggest the purity of the staked multilayer. Since the oxygen content cannot be quantified with the EDS (both substrate –SiO_2 and specimen layer SnO_2 contain oxygen), therefore a correct estimation of Au is not concluded using EDS.

XAS and XES studies

The O *K*-edge XAS spectra of the stacked TCO multilayer were measured in both surface-sensitive TEY and bulk-sensitive TFY modes. Comparison of their characteristic features to those of SnO

RSC Advances Accepted Manuscript

and SnO_2 powder reference samples (Fig. 3a) shows the surface region to be SnO, with additional spectral features evident from the TFY. This is further verified by the Sn M_{45}-edge TEY spectra (Fig. 3b) which are consistent with the O *K*-edge spectra showing a SnO-rich phase at the surface. Spectral features observed in the low energy regions of the O *K*–edge XAS in Fig. 3a are generated due to excitation from the O 1*s* core level into primarily O 2*p*-Sn 5*s* hybridized states,[24] which form the bottom of the conduction band. The second region at higher energies is composed mainly of O 2*p*-Sn 5*p* hybridized states in SnO and SnO_2.[24-26] The spectral peaks in the TFY spectrum of the TCO multilayer can be compared to XAS results of SnO_2 films deposited by atomic layer deposition (ALD)from Choi *et al.*[25] The line shape of the O 2*p*-Sn 5*s* peak at 534.5 eV and the energy splitting between this peak and the first peak in the O 2*p*-Sn 5*p* series (~2 eV), agrees with XAS of ALD films exhibiting an amorphous SnO_2 crystal structure.[25]

The peak at 534.5 eV in the TCO multilayer also indicates SnO_2 by its energy location. Similarly the first two sharper peaks *a* and *b* have similar energy splitting to the corresponding peaks in the SnO_2 reference sample (~1.2 eV). These details together indicate a dominant phase of SnO with small amount of SnO_2 below the surface that is amorphous in nature. The TCO multilayer structure including Au in a sandwich structure may also promote overlap between O-2*p* and Au-5*d*6*s* orbitals and increase the density of conduction band states. This overlap may contribute to the increased intensity of higher energy features in the range of 535-540 eV.[20]

A low energy shoulder feature under the bottom of the conduction band at 531.5 eV in TEY and TFY labeled as O_V is not typical of SnO or SnO_2 thin films or powders,[23-26] and may be due to the presence of oxygen vacancies. In the SnO/SnO_2 lattice of the TCO multilayer, oxygen vacancies introduced during the fabrication process could contribute to increased charge carrier transport and therefore conductivity by providing additional electronic states near the conduction band edge.

Non-resonant X-ray emission was also taken at the O *K*-edge to probe the density of valence band states, shown in Fig. 3c.Open blue circles show the raw XES spectrum overlaid with a smoothed line using 10 point FFT smoothing, which is used for the second derivative. From McLeod *et al.*,[24] the contribution of Sn 5*d* states to the top valence band is much greater for the $5s^0$ oxides (SnO_2) than the $5s^2$ oxides (SnO). In $5s^0$ oxides the top of the valence band is dominated by a sharp distribution of O 2*p* states strongly hybridized with these Sn 5*d* states, extending ~2.5 eV into the valence band from the Fermi level.[24] In $5s^2$ oxides, specifically SnO, a hybridization occurs between O 2*p* and Sn 5*s* states at the valence band edge, while the top and middle of the valence band are largely dominated by O 2*p* states. By contrast to SnO_2, the top of valence band of SnO exhibits a much broader distribution of states extending across ~5 eV.[24] The XES of the TCO multilayer shows a broad distribution of states near the top of the valence band (region *c* in Fig. 3d), indicating an SnO structure. From further comparison to experimental measurements in Ref. 24, near the middle of the valence band in the region labeled *e* an additional peak may be resolved in pure SnO that arises from O2*p*-Sn 5*s* states. The broadening of this feature such that it cannot be resolved as in the case of the TCO multilayer shows disorder in the SnO lattice due to the amorphous SnO/SnO_2 phase. A similar smearing of valence band features *d* and *e* has been observed for SnO_2 thin films below 220 nm in thickness, and was attributed to oxygen vacancies in that films.[26]

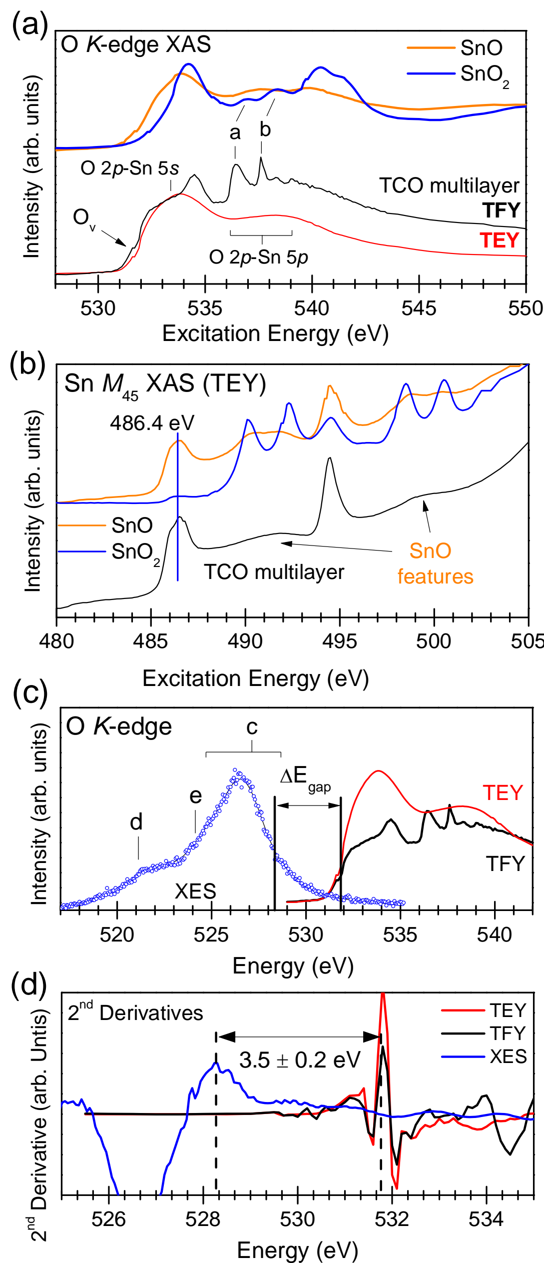

Fig.3 (a) O *K*-edge X-ray absorption spectra of SnO and SnO_2 reference samples along with the stacked TCO multilayer measured in TEY/TFY modes. (b) Sn *M*-edge spectra for the TCO multilayer compared to references, and (c) XES and XAS of the O *K*-edge where XES displays a valence band line shape indicating SnO. (d) The magnitude of the band gap energy is determined using second derivatives to be 3.5 ± 0.2 eV.

RSC Advances Accepted Manuscript

This journal is © The Royal Society of Chemistry 20xx

The band gap in SnO/SnO_2 can be determined from O *K*-edge measurements plotted on a common energy scale as in Fig. 3c.[24,25] When the second derivative is plotted the distance between the highest-energy peak of the XES derivative and the lowest-energy peak of the XAS derivative is determined to be the band gap energy splitting. This method provides a quantitative measurement of band gap energy without use of line fitting to the valence and conduction band edges. The second derivatives for O *K*-edge XES and XAS of the TCO multilayer are shown in Fig. 3d, and find the TCO multilayer band gap to be 3.5 eV ± 0.2 eV, which is larger than the reported band gap range of 2.5-3.0 eV for SnO.[23,27] This result is significant because it indicates that even though the films contain proportionally more SnO compared to SnO_2, the band gap matches more closely to that of SnO_2 (3.6 eV).[23]The SnO band structure and band gap energy are altered by the presence of a mixed phase with amorphous $SnO_2$and oxygen vacancies in a way that may be advantageous for device applications. A large band gap energy commonly results in higher transmittance in the visible range, while a metal rich SnO/SnO_2 phase may serve to lower resistivity of the TCO multilayer compared to pure metal oxide films.

RBS study

Fig. 4 shows the RBS spectrum and RUMP-fitted profile of the stacked multilayer.[28] This spectrum indicates the distinct elemental peaks associated with Sn, O, Au and Si. The thickness of structure is calculated with the help of this fitted profile. The estimated values are SnO_x(35nm)/Au(5.2nm)/SnO_x(35nm) with composition of SnO_x layer as: 0.575 of O and 0.425 of Sn. This suggests the formation of SnO (which is consistent with results from the XAS investigations) with pure Au in the sandwich layer.

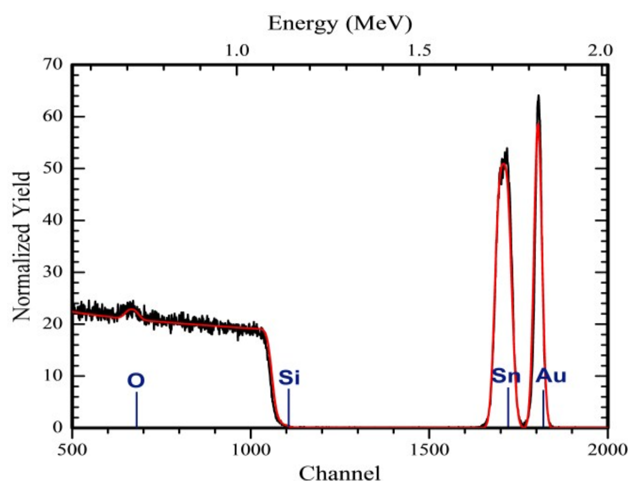

Fig.4 RBS spectrum along with fitted profile of the stacked multilayer. The peaks assigned for Sn and Au are seen at higher channels and Si and O are also seen at lower channels.

UV-Vis and Raman spectroscopy

The optical properties of the stacked multilayer recorded from a UV-Vis spectrophotometer are presented in Fig. 5 exhibiting nearly constant values for transmittance, absorbance and reflectance beyond 475 nm of incoming radiation (0.83, 0.08 and 0.09, respectively). The typical value of transparency for a commercially available ITO slide from Sigma-Aldrich (Product Number:703184, CAS Number:50926-11-9) is 0.84 (surface resistivity 30-60 Ω/*sq* and refractive index 1.517) which is quite near to the value obtained from this stacked multilayer. This transmittance value is better as compared to other reports for SnO on quartz substrates by Liang *et al.*[16], The ITO, ITO/Au/ITO and ITO/Cu/ITO on polycarbonate substrates reported by Lee *et al.*[10] and Au-embedded F-doped SnO_2 on glass substrates reported by Chew *et al.*[29]Higher transmittance and lower absorbance/reflectance are desirable properties for prospective use of these stacked multilayers as TCOs. Coating the metal film with a dielectric layer of higher refractive index is known to increase transmittance of the metal film with the dielectric layer acting as an antireflection film. Thin layer of polymer nano composite coated on metal as dielectric has been used to minimize the reflection of gold film increasing the optical properties of the system.[30]Hence enhanced optical properties of proposed dielectric metal dielectric (DMD) structure in the entire visible region are a result of having metal oxide layers on both sides of Au metal layer.

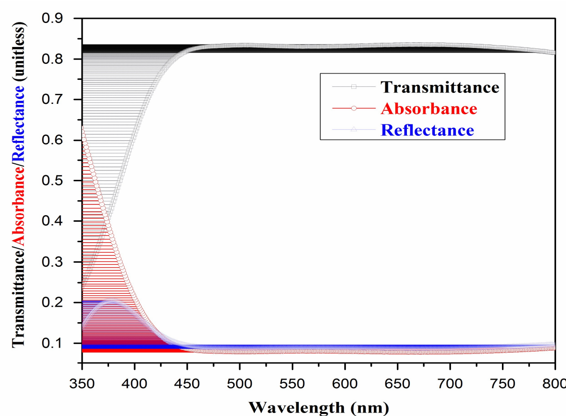

Fig.5 UV-Vis curve showing transmittance, absorbance and reflectance for stacked multilayer.

The Raman spectrum corresponding to stacked multilayer is shown in Fig. 6 (bold grey line) which includes multiple peaks deconvoluted from the Raman spectrum showing contribution from the transitions corresponding to vibrational levels. SnO_2 unit cell exhibits a total of 18 branches for the vibrational modes in first brillouin zone which results in four Raman active modes (A_{1g}, B_{1g}, B_{2g} and E_g).[31] The bottom curve in Fig.6 shows the residue to the fit. The peak structure is broad which is indicative of the formation of crystallites of very small size. The Raman shifts at 437 and 787 cm^{-1} (refer peaks *b* and *e* in Fig. 6) pertain to the characteristics E_g and B_{2g}modes of SnO_2.[32-33] All the other peaks (*a*,*c*,*d* and *f*) belong to the characteristic peaks of SiO_2[34] originating due to quartz substrate. The major contribution in the Raman spectrum is from

RSC Advances Accepted Manuscript

the quartz substrate which is due to small thickness and high transparency of the film.

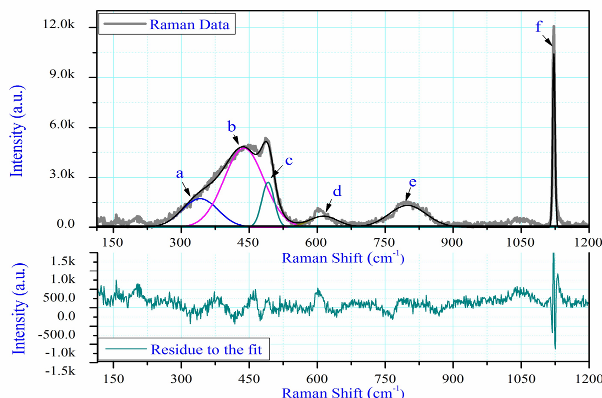

Fig.6 Raman spectrum of stacked multilayer.

Low temperature Hall study

Low temperature Hall effect and electrical resistivity measurements were carried out using Van der Pauw configuration. The variation of resistivity and sheet resistance for the temperature range of 80-340K is presented in Fig. 7.

The room temperature resistivity and sheet resistance for this stacked multilayer were $3.9\times10^{-4}\Omega\cdot$cm and 52 Ω/*sq*., respectively. The value of sheet resistance, 30-60 Ω/*sq*, is comparable to the commercial ITO slide from Sigma-Aldrich (Product Number:703184, CAS Number:50926-11-9). The resistivity values for SnO_x/Au/SnO_x specimen are lower than that for ITO films ($31.2\times10^{-4}\Omega\cdot$cm) reported by Lee *et el.*[10] and slightly higher toITO/Au/ITO and ITO/Cu/ITO structures showing resistivity of $0.56\times10^{-4}\Omega\cdot$cm and $1.51\times10^{-4}\Omega\cdot$cm, respectively.[10]

The conduction mechanisms of these stacked structures may be explained by considering a thin continuous layer of metal (Au) embedded between two oxide layers thereby forming a DMD structure. The total resistance of this coplanar configuration is generally given by: $1/R_{total}=1/R_{metal}+2/R_{oxide}$ with $R_{oxide}\approx1000R_{metal}$, so the $R_{total}\approx R_{metal}$. Therefore the conductivity is primarily due to embedded metal film and solely responsible for exhibiting such low values of resistivity as compared to single layer TCO. Moreover a critical thickness of the film is required to provide a continuous path for conduction of electron.[10,35-36]The room temperature resistivity and sheet resistance values for the staked multi layered structure are indicating a continuous metal inter layer.

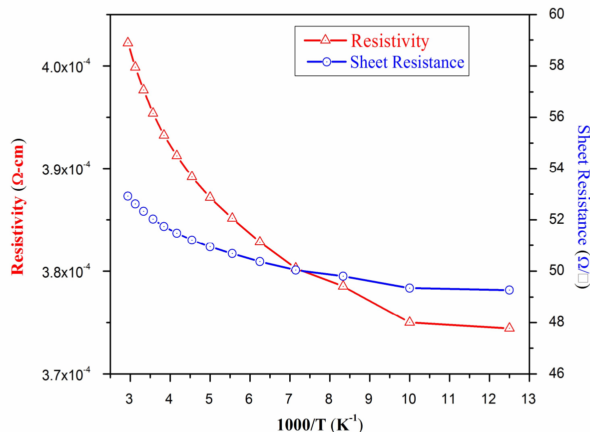

Fig.7 Electrical resistivity and sheet resistance as a function of reciprocal temperature.

Furthermore, the increase of both resistivity and sheet resistance with temperature is a typical characteristic of a degenerate semiconductor.[37]This behavior is resultant of increased concentration of metallic dopant which translates the semiconducting nature into metallic. There are numerous reports that support this argument in the literature e.g. Kim *etal.* for ITO films[37], *n*-type ZnO doped with Ga[38], Sb-doped *p*-type ZnO[39], highly B-doped ZnO films.[40] In the present system, increased resistivity and sheet resistance with increasing temperature can be attributed to effect of self-doping. The conclusions from XAS/XES and RBS investigations are indicative of formation of metal rich phase which would have produced the degenerate states thereby exhibiting a metal like behavior.

In addition to this, it is interesting to observe very high conductivity and low sheet resistance even at very low temperature. The stacked multilayer was shown to exhibit the values for resistivity and sheet resistance as $3.7\times10^{-4}\Omega$cm and 49 Ω/*sq*. at 80 K, respectively with a very small variation in both of these quantities up to 340K ($\delta\rho=0.2\times10^{-4}\Omega\cdot$cm and $\delta R_S=2.7$ Ω/*sq*.).

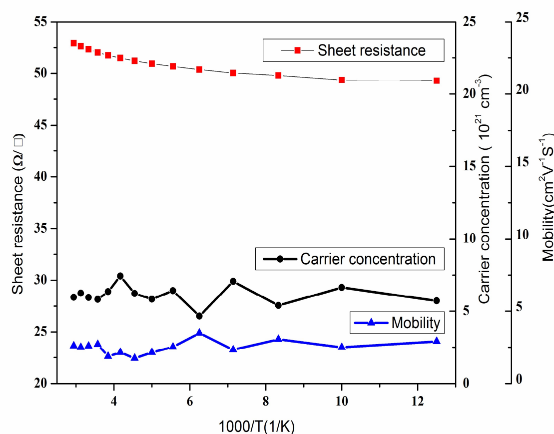

RSC Advances Accepted Manuscript

Fig.8 Sheet resistance, carrier concentration and mobility as a function of reciprocal temperature.

Conclusions

The stacked multilayered SnO_x/Au/SnO_x structure was deposited on quartz substrate using e-beam evaporation method for SnO_x and thermal evaporation method for *Au* layer to investigate its application as TCO. The XRD studies show an amorphous structure of the multilayer with AFM and SEM suggesting low roughness and flat morphology, respectively favoring the growth of further layers for technological applications. Both RBS and XAS investigations suggest formation of primarily SnO with evidence of a mixed phase containing SnO_2. Analysis of the spectral features in XAS and XES measurements confirms the presence of a mixed SnO/SnO_2phase. Amorphous SnO_2 within the SnO layer disrupts the SnO lattice and alters the electronic band structure. Combining XAS and XES measurements reveals a wide band gap energy (3.5 ± 0.2 eV), suitable for applications requiring high transparency in the visible range. Oxygen deficiency in SnO_x is indicated by RBS, and XAS confirms the presence of oxygen vacancies that can contribute to lower resistivity. The TCO characteristics resulting from the stacked multilayer were exhibiting high transparency (83% beyond 475 *nm*), lower sheet resistance (52Ω/*sq.*) and lower resistivity ($3.9\times10^{-4}\Omega\cdot$cm) which are comparable to that of standard ITO substrates. The increase in room temperature resistivity and sheet resistance with temperature is also suggesting metallic behavior which is attributed to the metal rich nature of the stacked multilayer. Such a multilayered structure with enhanced optical and electrical properties is proposed as a better replacement of the standard ITO substrates for opto-electronic applications.

Acknowledgements

The authors (V.S, R.V and K.S) are thankful for the research facilities provided by Inter University Accelerator Centre (IUAC), New Delhi (INDIA), Materials Research Centre (MRC) at MNIT Jaipur (INDIA), Wide Band Gap Semiconductor Lab at IIT-New Delhi and Canadian Light Source (CLS) at Saskatoon (CANADA). G.S.Chang acknowledges support from the Natural Sciences and Engineering Research Council of Canada (NSERC) and Canada Foundation for Innovation (CFI).

References

1 M. Nistor, E. Millon, C. Cachoncinlle, W. Seiler, N. Jedrecy, C. Hebert and J. Perrière, *J. Phys. D Appl. Phys.,* 2015, **48**, 195103.
2W. Cao, Y. Zheng, Z. Li, E. Wrzesniewski, W.T. Hammond and J. Xue, *J. Org. Electron.*, 2012, **13**, 2221–2228.
3T. Qiu, B. Luo, M. Liang, J. Ning, B. Wang, X. Li and L. Zhi, *Carbon,* 2015, **81**, 232–238.
4 K. Zilberberg, F. Gasse, R. Pagui, A. Polywka, A. Behrendt, S. Trost, R. Heiderhoff, P. G″rrn and T. Riedl, *Adv. Funct. Mater.*, 2014, **24**, 1671–1678.
5 H. Han, N.D. Theodore and T.L. Alford, *J. Appl. Phys.,* 2008, **103**, 013708.
6 J. Bellingham, W. Phillips and C. Adkins, *J. Mater. Sci.Lett.*,1992, **11**, 263–265.
7 M. Chen, Z. Pei, X. Wang, Y. Yu, X. Liu, C. Sun and L. Wen, *J. Phys. D Appl. Phys.*,2000, **33**, 2538.
8 K. Ellmer, *Nat. Photon.*, 2012, **6**, 809–817.
9 A. Indluru and T.L. Alford, *J. Appl. Phys.*,2009, **105**, 123528.
10 J.Y. Lee, J.W. Yang, J.H. Chae, J.H. Park, J.I. Choi, H.J. Park and D. Kim, *Opt.Commun.*,2009, **282**, 2362–2366.
11 S. Bansal, D.K. Pandya and S.C. Kashyap, *Appl. Phys. Lett.*,2014, **104**, 082108.
12 J. Dominguez, L. Fu and X. Pan, *Appl. Phys. Let.*,2001, **79**, 614–616.
13 A. Bou, P. Torchio, D. Barakel, F. Thierry, A. Sangar, P.Y. Thoulon and M. Ricci, *J. Appl. Phys.*,2014, **116**, 023105.
14 S. Yu, C. Jia, H. Zheng, L. Ding and W. Zhang, *Mater. Lett.*, 2012, **85**, 68–70.
15 Z.R. Li and H. Meng, *CRC, Boca Raton*, 2007.
16 L.Y. Liang, Z.M. Liu, H.T. Cao and X.Q. Pan, *ACS Appl. Mater. Interfaces.*, 2010, **2**, 1060–1065.
17 Y.H. Tak, K.B. Kim, H.G. Park, K.H. Lee and J.R. Lee, *Thin Solid Films*, 2002, **411**, 12–16.
18 C.X. Kronawitter, M. Kapilashrami, J.R. Bakke, S.F. Bent, C.H. Chuang, W.F. Pong, J. Guo, L. Vayssieres and S.S Mao, *Phys. Rev.* B, 2012, **85**, 125109.
19 K.G. Godinho, A. Walsh and G.W. Watson, *J. Phys. Chem. C*, 2008, 113, 439–448.
20 D.Y. Cho, S.I. Na, K.B. Chung and H.K. Kim, *Appl. Surf. Sci.*, 2015, **347**, 88–95.
21 M. Kapilashrami, C.X. Kronawitter, T. Törndahl, J. Lindahl, A. Hultqvist, W.C. Wang, C.L. Chang and S.S. Mao, *J. Phys. Chem. Chem. Phys.*, 2012, **14**, 10154–10159.
22 C.A. Schneider, W.S. Rasband and K.W. Eliceiri, *Nat. Methods* 2012, **9**, 671–675.
23C. McGuinness, C. B. Stagarescu, P. J. Ryan, J. E. Downes, D. Fu, K. E. Smith, R. G. Egdell. *Phys. Rev. B*, 2003, **68**, 165104.
24 J. A. McLeod, N. A. Skorikov, L. D. Finkelstein, E. Z. Kurmaev, A. Moewes, *J. Phys. Chem. C.*, 2012, **116**, 24248–24254.
25.D. Choi, W.J. Maeng, J.-S. Park. *Appl. Surf. Sci.,* 2014,**313**, 585–590.
26 G. S. Chang, J. Forrest, E. Z. Kurmaev, A. N. Morozovska, M. D. Glinchuk, J. A. McLeod, A. Moewes, T. P. Surkova, N. H. Hong. *Phys. Rev. B.* 2012,**85**, 165319.
27 S. Das and V. Jayaraman, *Prog.Mater. Sci.*, 2014, **66**, 112 – 255.
28 L. R. Doolittle, *Nucl.Instrum.Meth.* B, 1985, **9**, 344–351.
29 C.K. Chew, C. Salcianu, P. Bishop, C. J. Carmalt and I.P. Parkin, *J.Mater. Chem.* C, 2015, **3**, 1118-1125.
30 M. Elbahri, M. K. Hedayati, V.S.K. Chakravadhanula, M. Jamali, T. Strunkus, V. Zaporojtchenko and F. Faupel, *Adv. Mater.*, 2011, **23**, 1993–1997.
31 A. Dieguez, A. Romano-Rodrıguez, A. Vila and J.R. Morante, *J. Appl. Phys.*,2001, **90**, 1550–1557.
32 E. Fazio, F. Neri, S. Savasta, S. Spadaro and S. Trusso, *Phys. Rev. B*,2012, **85**, 195423.
33 Q.-H. Wu, J. Song and J. Li, *Surf. Inter. Anal.*,2008, **40**, 1488–1492.
34 T.F. Cooney, E. R. D. Scott, A.N. Krot, S.K. Sharma and A. Yamaguchi, *Am. Mineral.*,1999, **84**, 1569–1576.
35 Z. Xue, X. Liu, N. Zang, H. Chen, X. Zheng, H. Wang and X. Guo, *ACS Appl. Mater. Interfaces.*, 2014, **6**, 16403-16408.

RSC Advances Accepted Manuscript

36 K. Sivaramakrishnan, N.D. Theodore, J.F.Moulder and T. L. Alford, *J. Appl. Phys.*, 2009, **106**, 63510, 1–8.
37 H. Kim, C.M. Gilmore, A. PiquÃl', J.S. Horwitz, H. Mattoussi, H. Murata, Z.H. Kafafi and D.B. Chrisey, *J. Appl. Phys.*, 1999, **86**, 6451–6461.
38 M. Joseph, H. Tabata, H. Saeki, K. Ueda and T. Kawai, *Physica B*, 2001, **302**, 140–148.
39 F.X. Xiu, Z. Yang, L.J. Mandalapu, D.T. Zhao, J.L. Liu and W.P. Beyermann, *Appl. Phys. Lett.*,2005, **87**, 152101–152101.
40 S.Y. Myong, J. Steinhauser, R. Schlüchter, S. Faÿ, E. Vallat-Sauvain, A. Shah, C. Ballif and A. Rüfenacht, *Sol. Energ. Mat. Sol C*,2007, **91**, 1269–1274.

RSC Advances Accepted Manuscript

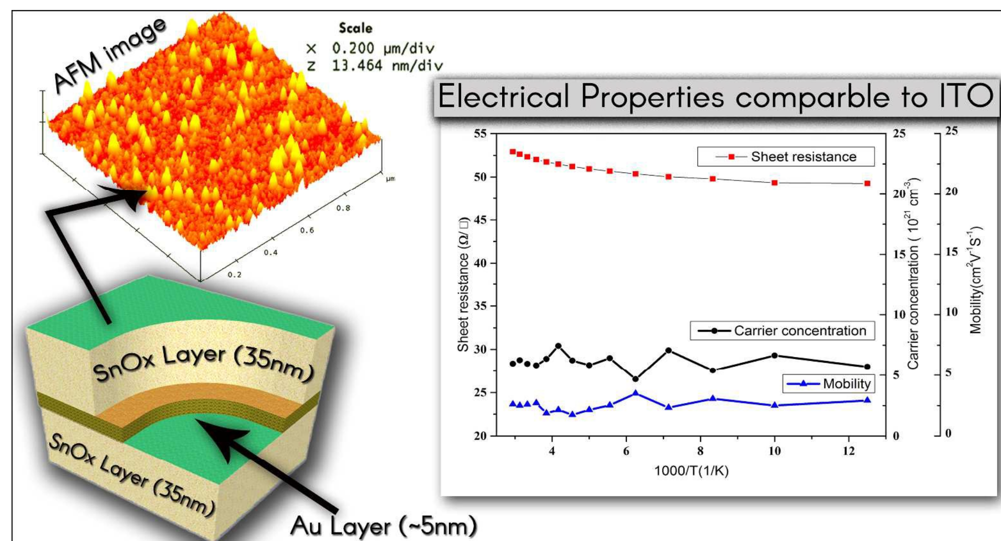

247x133mm (300 x 300 DPI)

RSC Advances Accepted Manuscript